ARCHIVES OF ELECTRICAL ENGINEERING VOL. 71(3), pp. 559–579 (2022)

DOI 10.24425/aee.2022.141671

Current limiting algorithm for three-phase grid-connected inverters

THO QUANG TRAN

Hochiminh City University of Technology and Education
Vietnam
e-mail: thotq@hcmute.edu.vn

(Received: 27.06.2021, revised: 03.02.2022)

Abstract: Grid-connected inverters are commonly used in systems of renewable energy to convert this energy source into AC power with parameters suitable for connection to the grid. In the normal operating conditions, the grid-connected inverters mainly generate active power to the grid. However, when a voltage sag or voltage imbalance occurs, the grid voltage imbalance in the conventional control methods causes negative sequence components and increases the output current magnitude of inverters. The increase of current can damage power semiconductor devices. This paper presents a strategy to limit the current magnitude of inverters under unbalanced grid voltage conditions. In this strategy, a multiple-complex-coefficient filter is used to eliminate the negative sequence voltage components. This method does not require any additional hardware. A three-phase grid-connected photovoltaic inverter system using a solar array of 20 kWp is also used for the survey. The effectiveness has been validated when comparing the simulation results on Matlab/Simulink of the proposed method with those of the conventional method.

Key words: current limitation, negative sequences, reactive power compensation, three-phase grid-connected inverters, unbalanced voltages

1. Introduction

The demand for electricity from renewable energies such as wind power and solar power is increasing due to their sustainability and environmental friendliness. However, the dependence on weather makes these renewable energy sources unstable. Therefore, to become an efficient power source with high quality, these energy sources need to be connected to the power grid. At that time, the grid-connected inverters using power semiconductor devices [1–3] are often adopted

© 2022. The Author(s). This is an open-access article distributed under the terms of the Creative Commons Attribution-NonCommercial-NoDerivatives License (CC BY-NC-ND 4.0, https://creativecommons.org/licenses/by-nc-nd/4.0/), which permits use, distribution, and reproduction in any medium, provided that the Article is properly cited, the use is non-commercial, and no modifications or adaptations are made.

www.czasopisma.pan.pl PAN POLSKA AKADEMIA NAUK www.journals.pan.pl

to convert these energy sources into the ac power with suitable parameters to connect the power grid.

Under normal operating conditions, the grid-connected inverters essentially generate the active power into the network. This active power is often lower than the rated value and the inverter current magnitude is also lower than the rated current. However, when the faults such as voltage sag and imbalance happen, the inverters must have the ability to support the power system [4–8] by compensating the reactive power for the power grid according to the grid codes [9–11]. The voltage imbalance causes the negative sequence voltage components to appear [12–14]. This makes the power generation ability of inverters decrease. In the conventional inverters, the voltage imbalance causes the current magnitude of power semiconductor devices to increase because the inverter output power is kept at the rated apparent power [6, 15]. The increase of current magnitude can cause over-current and damage the power devices of inverters.

There are many solutions published to control the grid-connected inverters under the voltage imbalance [17, 18]. However, these methods have only considered the current balance among the phases to reduce the active power at the DC side, they have not considered the over-current of the power devices. In addition, these methods have used additional power devices, which increase the cost and complexity of the control. Although the hysteresis control technique in [19] has been based on the power-states table and the instantaneous power theory [20] to control powers, it has not been applied to a specific grid-connected photovoltaic inverter system under grid voltage imbalance. Normally, the delta connection of transformers is also used to lock zero-sequence components [21]. However, this connection can cause overvoltage when a single-phase fault happens. In order to solve this problem, a method proposed in [22] has used the instantaneous power transformation to improve the transfer of power and eliminate the power oscillations. To detect the positive sequence components in the synchronous frame, the methods in [5, 23, 24] have also been proposed, however, their obstacles are slow response and difficult calculation. Moreover, the significant oscillation of active power at the DC side can affect the durability of the solar panels.

The technique in [25] uses the linear model of the synchronous rotating frame (SRF) phase-locked loop and the multiple-complex coefficient-filter (MCCF) to extract the positive and negative sequence components. However, the magnitude of the extracted positive sequence component is not decreased when the grid voltage imbalance occurs. The technique in [26] using the MCCF and moving average filter also has the magnitude of positive sequence components unchanged after the voltage imbalance occurs. The PLL in [27] using the MCCF to eliminate the selective harmonics has been applied to an active power filter. Thus, these PLL techniques have not been applied to solve the issues of over-current for the specific grid-connected photovoltaic inverter systems.

In the meanwhile, the over-current of inverters has not been considered. The over-current of semiconductor power devices is one of the most important reasons and can damage the inverters. In most of distributed generations [28] using renewable energy sources, the inverter systems are used to connect grids. The conventional control methods of these inverters are usually based on the grid voltage parameters via a phase-locked loop (PLL) to synchronize with the grid. Once an unbalanced voltage fault occurs, conventional PLLs cannot recognize the presence of negative sequence voltage components, which makes the real magnitude of the grid voltage decrease. Therefore, the apparent power generated into the grid is not adequately adjusted to the

decrease. This can cause over-current. In addition, these PLLs make the inverters significantly generate the current harmonics into the grid and affect the stability of the power system [29]. Thus, they have an adverse impact on the power quality of the power system. To ensure the safe operation and transmission of the electricity, the grid codes have been issued by the grid operation departments [9, 11–29], in which the regulations of reactive power generation are also required to support the grid when the voltage sag and imbalance happen.

This paper proposes a calculation method for limiting the current magnitude of grid-connected inverters in operation under voltage imbalance. In the proposed method, a phase-locked loop and a multiple-complex-coefficient filter [30] are used to extract the positive sequence components of the grid voltage and reject the adverse effects of the negative sequence voltages. Moreover, a power calculation method is also useful when voltage imbalance occurs. This method does not require any additional hardware. The calculation method of conventional inverters is showed in Section 2. The proposed method is presented in Section 3. The simulation results and discussion of the two methods are showed in Section 4. The effectiveness of the proposed method is concluded in Section 5.

2. Power control under voltage imbalance

2.1. Phase-locked loop (PLL)

In a grid-connected inverter system using the principle diagram showed in Fig. 1, the control of this inverter is based on the voltage parameters estimated by a conventional PLL, as showed in Fig. 2, where V_{sa}, V_{sb}, and V_{sc} are the phase voltages of the grid. The voltages V_α and V_β are transformed according to the Clarke matrix in (1). Then, the magnitude of the grid voltage $V_{\max}$

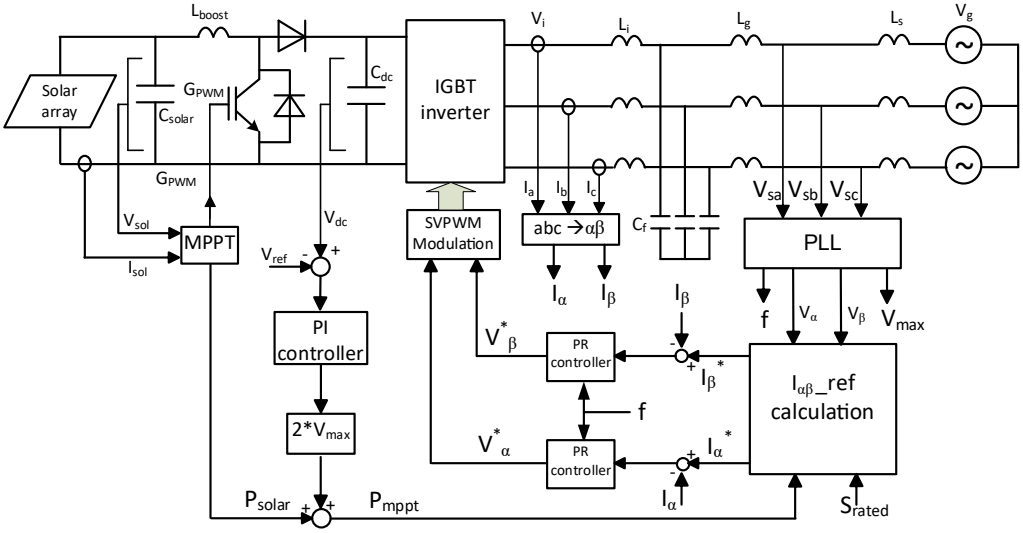

Fig. 1. Principle diagram of a grid-connected inverter system

is defined as in (2). The waveforms of the voltages at a fundamental frequency of 50 Hz are also showed in Fig. 3, and surveyed in the intervals of time from 0.24–0.4 s.

$$\begin{bmatrix} V_\alpha \\ V_\beta \end{bmatrix} = \frac{2}{3} \begin{bmatrix} 1 & -1/2 & -1/2 \\ 0 & -\sqrt{3}/2 & \sqrt{3}/2 \end{bmatrix} \begin{bmatrix} V_{sa} \\ V_{sb} \\ V_{sc} \end{bmatrix}, \tag{1}$$

$$V_{\max} = \sqrt{V_\alpha^2 + V_\beta^2}\,. \tag{2}$$

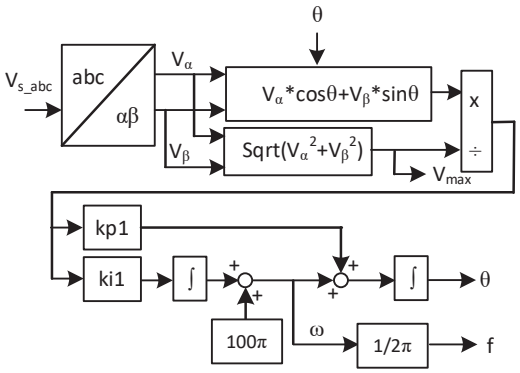

Fig. 2. Principle of a conventional PLL

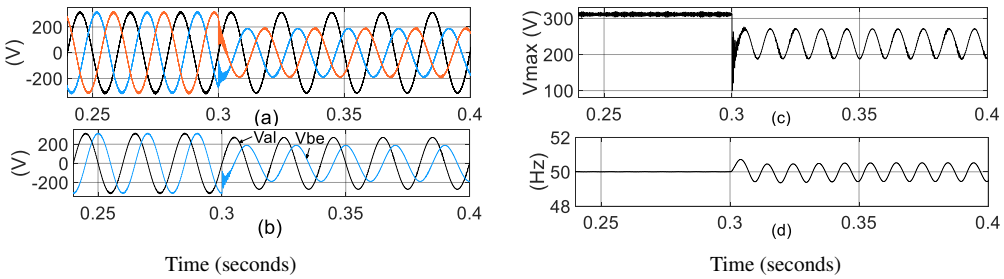

Fig. 3. Estimated responses when imbalance happens at 0.3 s (voltage magnitudes of the phases B and C are equal to 60 per cent of the rated value): three phase voltages of the grid (a); V_α and V_β (b); $V_{\max}$ (c); grid frequency (d)

In the first interval, 0.24–0.3 s, the voltages of three phases are balanced in the normal operation and showed in Fig. 3(a). This helps the voltage magnitudes of V_α and V_β balance in Fig. 3(b). Then, the estimated by the PLL parameters of the grid voltage, including the magnitude $V_{\max}$ and grid frequency f, are also showed in Figs. 3(c)–3(d). However, after 0.3 s, the voltage magnitudes of phases B and C are decreased to 60% of the rated value in Fig. 3(a). This also causes the imbalance of the voltage magnitudes V_α and V_β in Fig. 3(b) after 0.3 s. Then, the estimated voltage parameters in Figs. 3(c)–3(d) are significantly oscillated. These oscillations cause the inverters to generate harmonics into the grid and affect the stability of the power system.

www.czasopisma.pan.pl PAN POLSKA AKADEMIA NAUK www.journals.pan.pl

2.2. Power control

Under the normal operation, the active power P is always extracted from the renewable energy sources with the maximum value P_{mppt} by the maximum power point tracker (MPPT) and the reactive power Q is always as zero. These values are used as the reference powers to generate into the grid. However, when the grid voltage magnitude is lower than 90% of the rated value, the inverters must generate the reactive power Q into the grid as in (4) and in Fig. 4, to support the power system [31, 32].

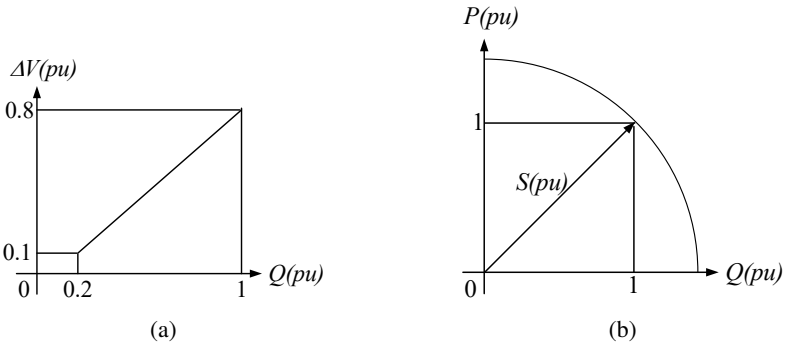

Fig. 4. Regulation of reactive power generation: reactive power versus the voltage drop (a); constraint of power quantities (b)

$$\Delta V(\%) = \frac{V_{\max n} - V_{\max}}{V_{\max n}} \cdot 100\%, \tag{3}$$

$$Q = \sqrt{S_{\text{rated}}^2 - P^2}, \tag{4}$$

where $V_{\max n}$ is the rated phase voltage magnitude and $V_{\max}$ is the voltage magnitude of the grid estimated by the PLL. $\Delta V(\%)$ is the voltage drop and S_{rated} is the rated apparent power of inverters.

The reference currents are defined as follows:

$$\begin{bmatrix} i_{\alpha\_\text{ref}} \\ i_{\beta\_\text{ref}} \end{bmatrix} = \frac{1}{V_\alpha^2 + V_\beta^2} \begin{bmatrix} V_\alpha & -V_\beta \\ V_\beta & V_\alpha \end{bmatrix} \begin{bmatrix} P \\ Q \end{bmatrix}. \tag{5}$$

3. Proposed method

3.1. Analysis of voltage imbalance

Under the normal operation with the balanced voltage, three phase voltages of a 3-wire 3-phase system only have the positive sequence components and are described as follows:

$$\left.\begin{aligned} V_{sa} &= V^+ \sin\left(\omega t + \varphi^+\right) \\ V_{sb} &= V^+ \sin\left(\omega t - 2\pi/3 + \varphi^+\right) \\ V_{sc} &= V^+ \sin\left(\omega t + 2\pi/3 + \varphi^+\right) \end{aligned}\right\}. \tag{6}$$

www.czasopisma.pan.pl PAN POLSKA AKADEMIA NAUK www.journals.pan.pl

When the voltage imbalance happens, the zero-sequence component does not exist for the 3-wire 3-phase system in the static reference frame. However, the negative sequence components appear and are described as follow:

$$\left.\begin{aligned} V_{sa} &= V^{+}\sin\left(\omega t+\varphi^{+}\right)+V^{-}\sin\left(\omega t+\varphi^{-}\right)\\ V_{sb} &= V^{+}\sin\left(\omega t-2\pi/3+\varphi^{+}\right)+V^{-}\sin\left(\omega t+2\pi/3+\varphi^{-}\right)\\ V_{sc} &= V^{+}\sin\left(\omega t+2\pi/3+\varphi^{+}\right)+V^{-}\sin\left(\omega t-2\pi/3+\varphi^{-}\right)\end{aligned}\right\}. \tag{7}$$

In addition, three phase currents also contain the negative sequence components and are defined as:

$$\left.\begin{aligned} I_{a} &= I^{+}\sin\left(\omega t+\delta^{+}\right)+I^{-}\sin\left(\omega t+\delta^{-}\right)\\ I_{b} &= I^{+}\sin\left(\omega t-2\pi/3+\delta^{+}\right)+I^{-}\sin\left(\omega t+2\pi/3+\delta^{-}\right)\\ I_{c} &= I^{+}\sin\left(\omega t+2\pi/3+\delta^{+}\right)+I^{-}\sin\left(\omega t-2\pi/3+\delta^{-}\right)\end{aligned}\right\}, \tag{8}$$

where V^{+} and V^{-} are the voltage magnitudes of the positive and negative sequences. I^{+} and I^{-} are the current magnitudes of the positive and negative sequences. φ^{+} and φ^{-} are the phase angles of the positive and negative sequence voltages. δ^{+} and δ^{-} are the phase angles of the positive and negative sequence currents, respectively. Then, the instantaneous apparent power s is also defined as follows:

$$s = v_{\alpha\beta}i^{*}_{\alpha\beta} = p + jq, \tag{9}$$

where $v_{\alpha\beta}$ is the voltage vector in the static reference frame and $i^{*}_{\alpha\beta}$ is the current vector of complex conjugates. p and q are the instantaneous active and reactive powers, respectively.

Under the balanced voltage condition, there is no oscillation in the active and reactive powers. However, when the voltage imbalance happens, the negative sequence components of the voltages and currents appear. Then, the apparent power will be defined as follows:

$$s = v_{\alpha\beta}i^{*}_{\alpha\beta} = \left(v^{+}_{\alpha\beta}+v^{-}_{\alpha\beta}\right)\left(i^{+}_{\alpha\beta}+i^{-}_{\alpha\beta}\right)* = p + jq, \tag{10}$$

with

$$v^{+}_{\alpha\beta} = \frac{1}{2}\begin{bmatrix} 1 & -e^{-j\pi/2}\\ e^{-j\pi/2} & 1\end{bmatrix} \tag{11}$$

and

$$v^{-}_{\alpha\beta} = \frac{1}{2}\begin{bmatrix} 1 & e^{-j\pi/2}\\ -e^{-j\pi/2} & 1\end{bmatrix}. \tag{12}$$

The current vectors are also defined similarly. Then, the active power p will be described as:

$$p = \left(V^{+}_{\alpha}I^{+}_{\alpha}+V^{+}_{\beta}I^{+}_{\beta}+V^{-}_{\alpha}I^{-}_{\alpha}+V^{-}_{\beta}I^{-}_{\beta}\right)+\left(V^{+}_{\alpha}I^{-}_{\alpha}+V^{+}_{\beta}I^{-}_{\beta}+V^{-}_{\alpha}I^{+}_{\alpha}+V^{-}_{\beta}I^{+}_{\beta}\right) = p_{\mathrm{con}}+p_{\mathrm{osc}}, \tag{13}$$

and the reactive power q is as follows:

$$q = \left(V^{+}_{\beta}I^{+}_{\alpha}-V^{+}_{\alpha}I^{+}_{\beta}+V^{-}_{\beta}I^{-}_{\alpha}-V^{-}_{\alpha}I^{-}_{\beta}\right)+\left(V^{+}_{\beta}I^{-}_{\alpha}-V^{+}_{\alpha}I^{-}_{\beta}+V^{-}_{\beta}I^{+}_{\alpha}-V^{-}_{\alpha}I^{+}_{\beta}\right) = q_{\mathrm{con}}+q_{\mathrm{osc}}. \tag{14}$$

Therefore, the active power consists of a constant component p_{con} and an oscillation one p_{osc}. Similarly, the reactive power also contains a constant component q_{con} and an oscillation component q_{osc}. According to (5), although the oscillation component of reactive power does not affect the DC side, it effects the AC currents. In addition, the oscillation of active power will adversely affect the DC side.

www.czasopisma.pan.pl PAN POLSKA AKADEMIA NAUK www.journals.pan.pl

3.2. Extraction of the positive sequence components

$$\begin{bmatrix} V_\alpha \\ V_\beta \end{bmatrix} = \begin{bmatrix} V_\alpha^+ \\ V_\beta^+ \end{bmatrix} + \begin{bmatrix} V_\alpha^- \\ V_\beta^- \end{bmatrix}. \tag{15}$$

There is no zero-sequence component in the 3-wire 3-phase system when the voltage imbalance happens. However, the negative sequence components will appear as in (15) and are illustrated in Fig. 5.

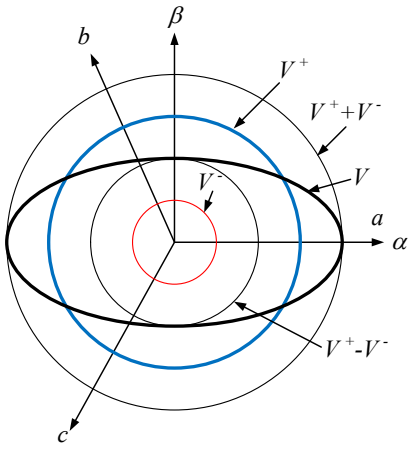

Fig. 5. Grid voltage V when having the negative sequence components

In (15), V_α^+ and V_α^- are the positive and negative sequence voltages in the real axis α, V_β^+ and V_β^- are the positive and negative sequence voltages in the image axis β. These voltages make the magnitude of the voltage vector V vary according to the trajectory of an ellipse. This ellipse has the semi-major axis as $V^+ + V^-$ and the semi-minor axis as $V^+ - V^-$.

To extract the negative sequence components, the decoupled double synchronous reference frame (DDSRF-PLL) in [33] uses low-pass filters. The dual second-order generalized integrator PLL (DSOGI-PLL) in [14] uses two SOGIs to extract negative and positive sequence components. It acts as a low-pass filter for the positive sequence and a notch filter for the negative-sequence. In addition, the DSOGI-FLL uses the trigonometric function $(\tan)^{-1}$ to calculate the theta angle. However, these techniques have only focused on the synchronization. They have not focused on the decreased magnitude of positive sequence grid voltage when the voltage imbalance happens. They have also not been applied to solve the over-current issue and the power change for a specific grid-connected photovoltaic inverter system.

In this paper, a multiple-complex-coefficient filter [27, 30] is proposed to extract positive sequence voltage components as in (16), and the detailed model of this filter on Matlab/Simulink is showed in Fig. 6. The positive sequence extractor (PSE) is used to detect the positive sequence voltages V_α^+ and V_β^+ in Fig. 6(a). The negative sequence extractor (NSE) is used to detect the positive sequence voltages V_α^- and V_β^- in Fig. 6(b). In (16), ω_c is the cut angular frequency. ω_0 is the estimated angular frequency and n is the harmonic order that needs to be extracted. In this

www.czasopisma.pan.pl PAN POLSKA AKADEMIA NAUK www.journals.pan.pl

paper, n as 1 (fundamental frequency) is chosen. The model of the proposed PLL using this filter is also showed in Fig. 7.

$$\begin{bmatrix} V^{+}_{\alpha\beta}(s) \\ V^{-}_{\alpha\beta}(s) \end{bmatrix} = V_{\alpha\beta}(s) \begin{bmatrix} \dfrac{\omega_c}{s - jn\omega_0 + \omega_c} \\ \dfrac{\omega_c}{s + jn\omega_0 + \omega_c} \end{bmatrix}. \tag{16}$$

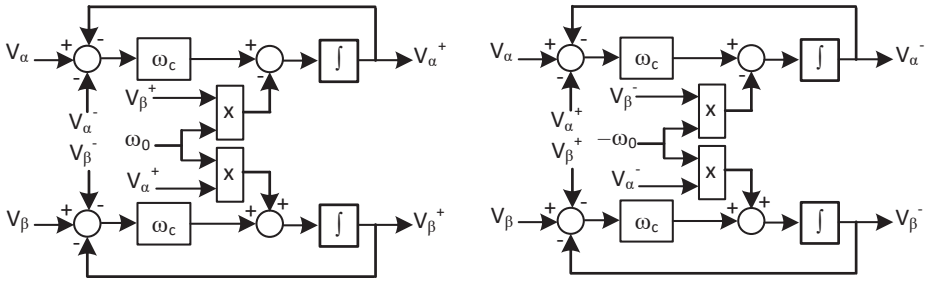

Fig. 6. The multiple-complex-coefficient filter model of extraction on Matlab/Simulink: the positive sequence extractor (a); the negative sequence extractor (b)

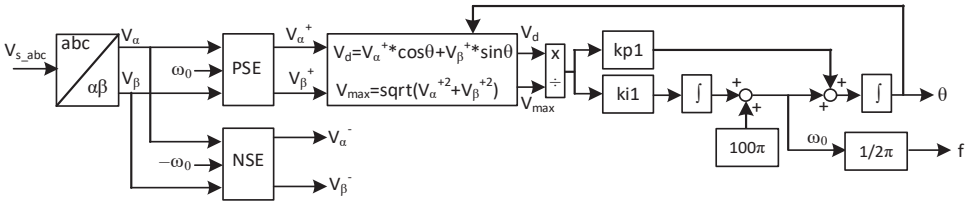

Fig. 7. The proposed PLL using the extraction of the positive sequence voltage components

The waveforms of the positive sequence voltage components and the negative ones are extracted by the proposed PLL from the grid voltage showed in Fig. 8, when the phase voltages, B and C, are decreased to 60% of the rated value at 0.3 s. Thus, under the grid voltage imbalance, the magnitudes of the positive sequence voltages were decreased while those of the negative ones were increased. The positive and negative sequence voltages will be used for calculating the reference powers and currents injected into the grid.

The control model using the proposed PLL is showed in Fig. 9, where the reference powers, currents I^{*}_{α}, and I^{*}_{β} are calculated based on the voltage components in the block proposed calculation of $I_{\alpha\beta\_\mathrm{ref}}$.

When the voltage imbalance happens, the positive sequence voltage magnitudes are decreased as in Fig. 8(b), after 0.3 s. Therefore, the new apparent power is also decreased and defined as follows:

$$S_{\mathrm{new}} = S_{\mathrm{rated}} \frac{\sqrt{\left|\left(V^{+2}_{\alpha} + V^{+2}_{\beta}\right) - \left(V^{-2}_{\alpha} + V^{-2}_{\beta}\right)\right|}}{V_{\max n}} = S_{\mathrm{rated}} \frac{V_{\mathrm{new}}}{V_{\max n}}, \tag{17}$$

where S_{new} is the new rated apparent power when appearing the negative sequence components. Then, the new voltage drop ΔV_{new} is also calculated as follows:

$$\Delta V_{\text{new}}(\%) = 100\% \frac{V_{\max n} - \sqrt{\left|\left(V_{\alpha}^{+2} + V_{\beta}^{+2}\right) - \left(V_{\alpha}^{-2} + V_{\beta}^{-2}\right)\right|}}{V_{\max n}}. \tag{18}$$

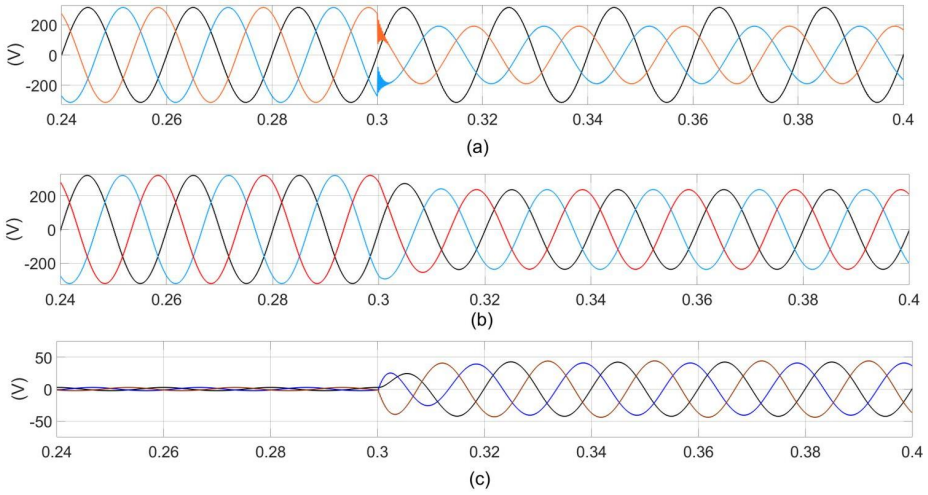

Fig. 8. Voltage waveforms: grid voltages (a); positive sequence voltage components (b); negative sequence voltage components (c)

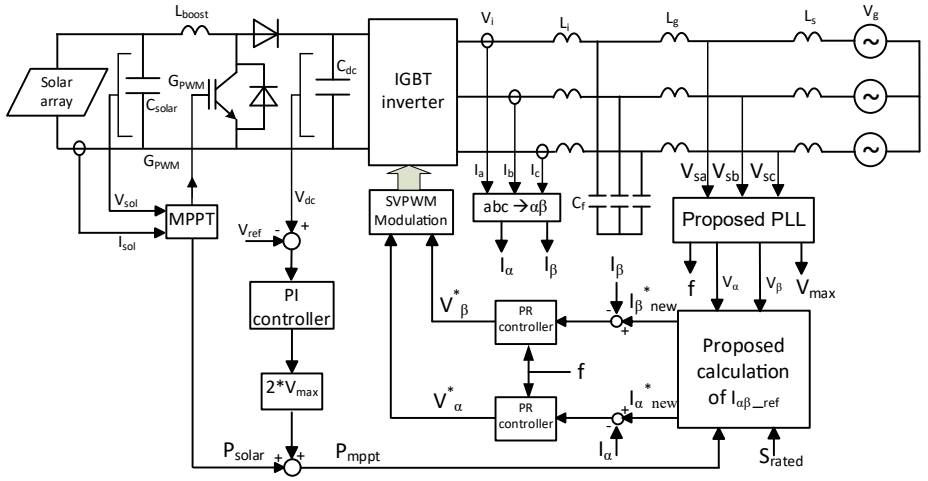

Fig. 9. The proposed control model

www.czasopisma.pan.pl PAN POLSKA AKADEMIA NAUK www.journals.pan.pl

Similarly, the reactive and active powers are also calculated as the following:

$$Q_{\text{ref}} = \begin{cases} 0 & \text{if } \Delta V_{\text{new}}(\%) \leq 10\% \\ \sqrt{2} S_{\text{new}} \cdot \Delta V_{\text{new}} & \text{if } \Delta V_{\text{new}}(\%) > 10\% \end{cases}, \tag{19}$$

$$P_{\text{new}} \leq \sqrt{S_{\text{new}}^2 - Q_{\text{ref}}^2}\,. \tag{20}$$

In reality, the renewable energy sources can vary with the weather. In some cases, the active power P_{mppt} from these sources can be greater than the permitted power P_{new}. Then, the reference active power is defined as follows:

$$P_{\text{ref}} = \begin{cases} P_{\text{new}} & \text{if } P_{\text{new}} \leq P_{\text{mppt}} \\ P_{\text{mppt}} & \text{if } P_{\text{new}} > P_{\text{mppt}} \end{cases}, \tag{21}$$

and the reference currents are calculated according to the reference powers and positive sequence voltages as follows:

$$\begin{bmatrix} i^*_{\alpha\_\text{new}} \\ i^*_{\beta\_\text{new}} \end{bmatrix} = \frac{1}{V_\alpha^{+2} + V_\beta^{+2}} \begin{bmatrix} P_{\text{ref}} & Q_{\text{ref}} \\ -Q_{\text{ref}} & P_{\text{ref}} \end{bmatrix} \begin{bmatrix} V_\beta^+ \\ V_\alpha^+ \end{bmatrix}. \tag{22}$$

This calculation helps inverter semiconductor power devices not be over-current. Then, the currents injected into the grid are regulated by proportional resonance (PR) controllers and the space vector pulse width modulation (SVPWM).

4. Results and discussion

4.1. Parameters setting

The system parameters are showed in Table 1, where the coefficients of controllers are defined based on the calculation method in [2]. The grid short-circuit apparent power is chosen as 4.5 MVA. The internal impedance of the grid source is chosen by the values of R_s and L_s in Table 1 so that the grid voltage THD is 1.05%. This voltage harmonic is similar to that of the source in the reality. A solar array consists of 11 parallel strings. Each string contains 6 series-connected modules of SUNPOWER-SPR-305E-WHT-D. Thus, the solar array gives a peak power of about 20.13 kWp. The characteristics of the solar array are showed in Fig. 10 with different irradiance levels at 25°C. The system parameters are also described in Table 1.

There are four intervals of time chosen to survey in this paper, from 0 to 1 s. In the first interval, 0–0.3 s, the grid phase voltages are balanced and frequency is at 50 Hz. In the second interval, 0.3–0.5 s, the grid phase voltage magnitudes, B and C, are decreased to 60% of the rated value that causes the imbalance, and frequency is still at 50 Hz. In the third interval, 0.5–0.7 s, the grid frequency steps from 50 Hz to 48 Hz occur at 0.5 s. The irradiance level of the solar array is 1000 W/m^2 in intervals from 0–0.7 s. In the last interval, 0.7–1 s, the irradiance level of the solar array is stepped to 500 W/m^2. In the rated voltage condition, with the rated apparent power S at 20 kVA, the rated current magnitude of the inverter injected into the grid is about 42 A. The surveyed results from 1–2 s, are also repeated from 0–1 s.

Table 1. System parameters

Parameter	Symbol	Value
Grid source voltage	V_g	$3 \cdot 380$ VAC
Grid source frequency	f_g	50 Hz
Resistor of the grid source	R_s	0.1 Ω
Inductor of the grid source	L_s	0.1 mH
Resistor of filter at the grid side	R_g	0.01 Ω
Inductor of filter at the grid side	L_g	0.01 mH
Resistor of filter at the inverter side	R_i	0.01 Ω
Inductor of filter at the inverter side	L_i	7.5 mH
Capacitor of filter	C_f	5 µF
DC voltage	V_{dc}	680 V
DC capacitor	C_{dc}	10 000 µF
Switching frequency	f_{svpwm}	10 kHz
Sample time of sensors	f_{sample}	10 kHz
Solar array power	P_{solar}	20 kWp
Coefficients of PI controller in PLL	$kp1$; $ki1$	222.1; 11974
Cut angular frequency	ω_c	$70\,\pi$ rad/s
Coefficients of DC voltage controller	kpdc; kidc	1; 0.05
Coefficients of PR controllers	kp; ki	0.21; 12

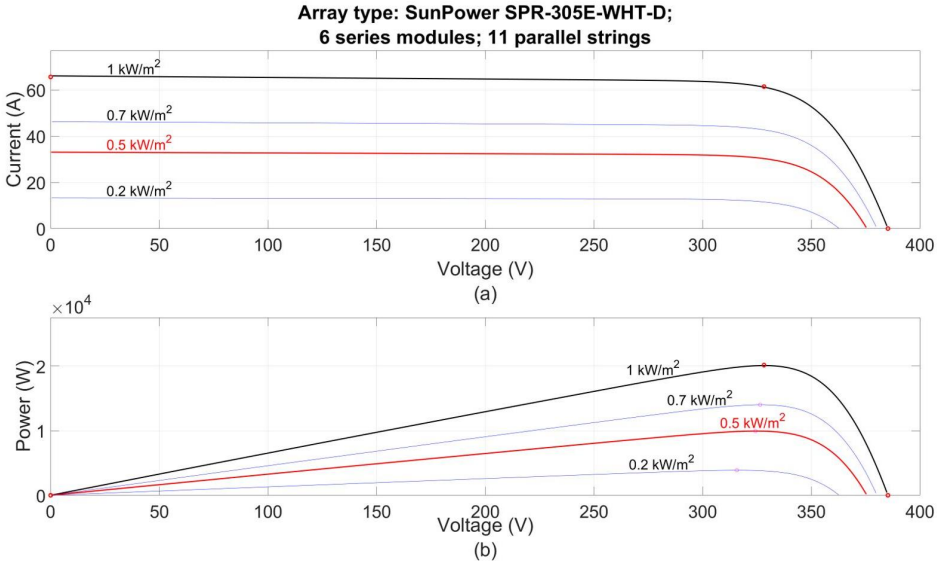

Fig. 10. The characteristics of the solar array: V-A curve (a); V-W curve (b)

The reference DC voltage is defined as follows:

$$V_{\text{ref}} = \frac{V_{L-L} \cdot \sqrt{2} \cdot K_v}{m} = \frac{380 \cdot \sqrt{2} \cdot 1.1}{0.866} \approx 680 \text{ V}, \tag{23}$$

where m is the modulation index and K_v is the factor depending on the voltage drop across the devices and filter.

4.2. Results and discussion

The surveyed results are showed in Figs. 11–19. In Fig. 11, the waveforms are the voltages of the grid source, the positive sequence components, and negative sequence components, respectively. They are also magnified in Fig. 12 from 0.28–0.6 s. The grid voltage imbalance

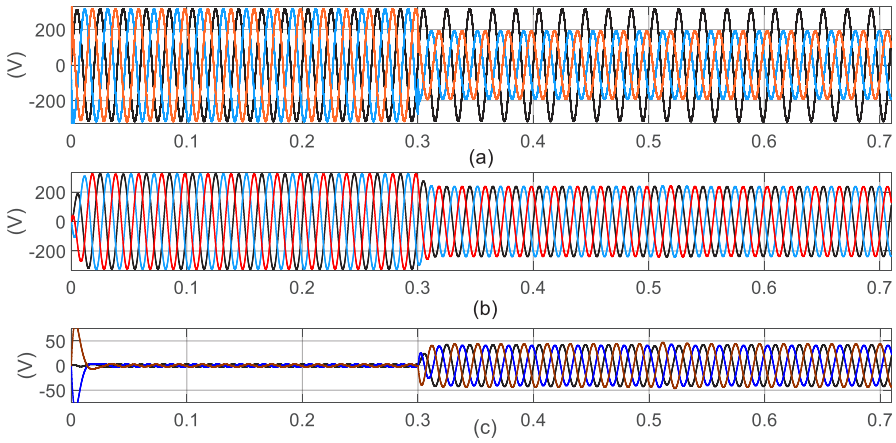

Fig. 11. Voltage waveforms: grid voltages (a); positive sequence voltages (b); negative sequence voltages (c)

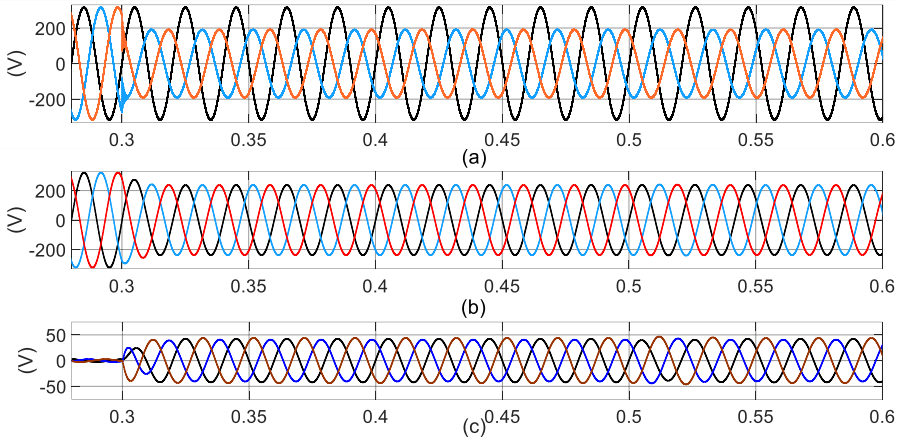

Fig. 12. Voltage waveforms magnified in the interval 0.28–0.6 s: grid voltages (a); positive sequence voltages (b); negative sequence voltages (c)

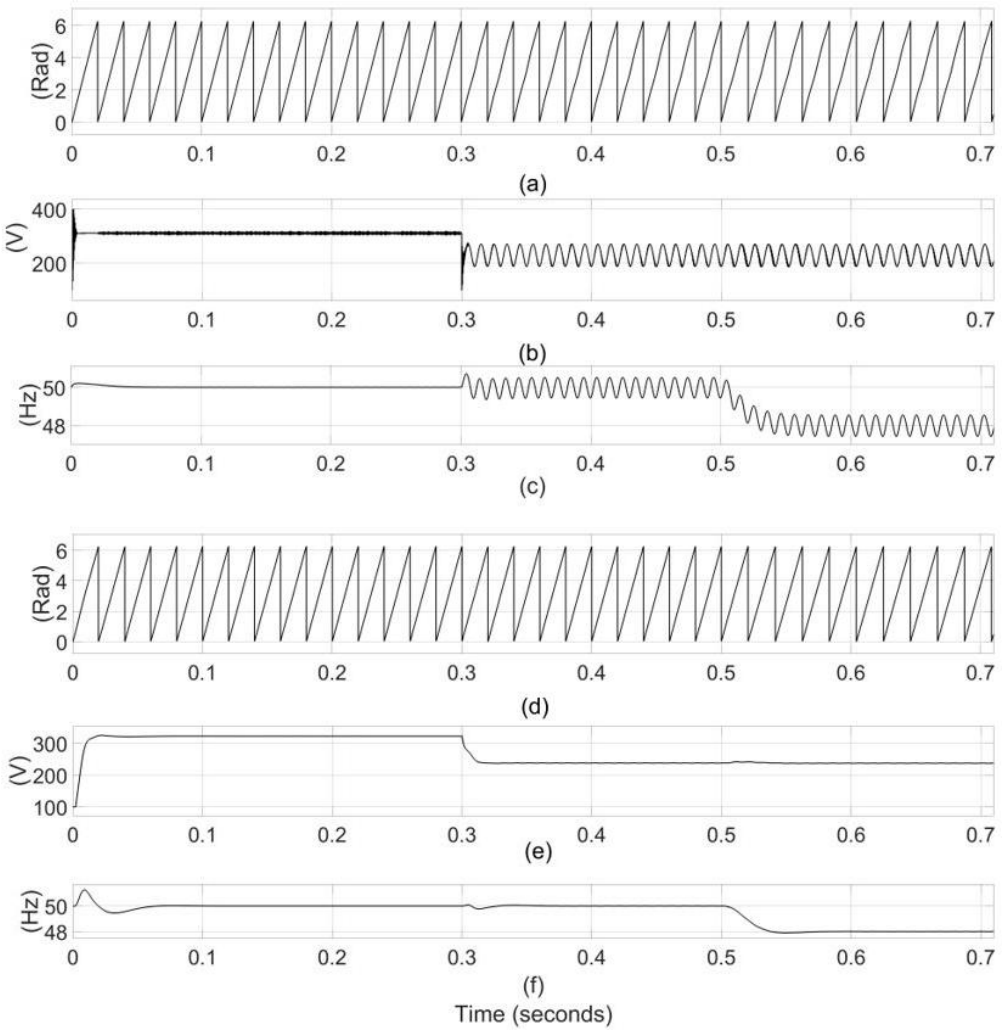

Fig. 13. Phase angle, magnitude, and frequency estimated by: the conventional PLL (a)–(c); the proposed PLL (d)–(f)

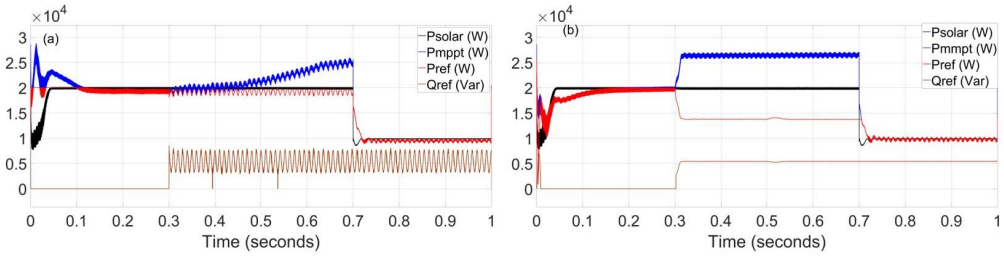

Fig. 14. Power responses: conventional method (a); proposed method (b)

happens at 0.3 s and is showed in Fig. 12(a). This makes the positive sequence voltage magnitude in Fig. 12(b) decrease. In addition, the negative sequence voltage also appears after 0.3 s, see Fig. 12(c).

In the first interval, 0–0.3 s (or 1–1.3 s), there is a similarity in the surveyed results between the two methods. However, the ripples in the estimated voltage magnitude in Fig. 13(b) are slightly high. This makes the current harmonics injected into the grid increase compared with those of the proposed method. After 0.3 s, the grid voltage imbalance happens. Then, for the conventional PLL, the appearance of the negative sequence voltages in Fig. 11(c) makes the estimated voltage magnitude and frequency in Figs. 13(b)–13(c) oscillate significantly. This also makes the reference powers in Fig. 14(a) oscillate, respectively. Consequently, the reference current magnitudes in Fig. 15(a) are unbalanced and exceed the rated value (42 A). These magnitudes have caused the over-current of the inverter. The current magnitudes injected into the grid are increased up to 72 A after 0.3 s and are showed in Figs. 16(a)–16(c), although the fundamental current magnitude is only 59.54 A in Fig. 18(b) and Tables 2 and 3. However, this value still exceeds the rated value (42 A). In addition, the current waveforms are distorted significantly and make the current THD values of the three phases increase up to 27.54% in Table 3.

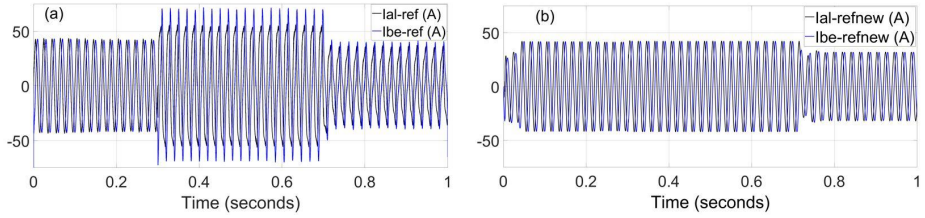

Fig. 15. Reference current responses: conventional method (a); proposed method (b)

Table 2. Fundamental current magnitude and current THD of phase C

Freq (Hz)	**At the instant (s)**	**Conventional method**		**Proposed method**	
		***I*peak (A)**	**THD (%)**	***I*peak (A)**	**THD (%)**
50	1.28	42.07	3.88	42.03	**1.99**
50	1.48	**59.54**	**19.05**	42.67	**1.45**
48	1.67	**59.77**	**18.94**	42.56	**1.44**
48	1.97	**33.74**	**23.69**	32.03	**2.81**

In the meanwhile, with the PLL of the proposed method, the estimated voltage magnitude and frequency in Figs. 13(e)–13(f) do not have any oscillation. Even when the grid frequency steps down to 48 Hz after 0.5 s. These estimated values are used to calculate the reference powers. As a result, there is no oscillation in these reference powers in Fig. 14(b). This helps the reference current magnitudes be balanced and not exceed the rated value as showed in Fig. 15(b). The quality of the estimated voltage parameters also helps the currents injected into the grid not exceed the rated limit in Figs. 16(d)–16(f).

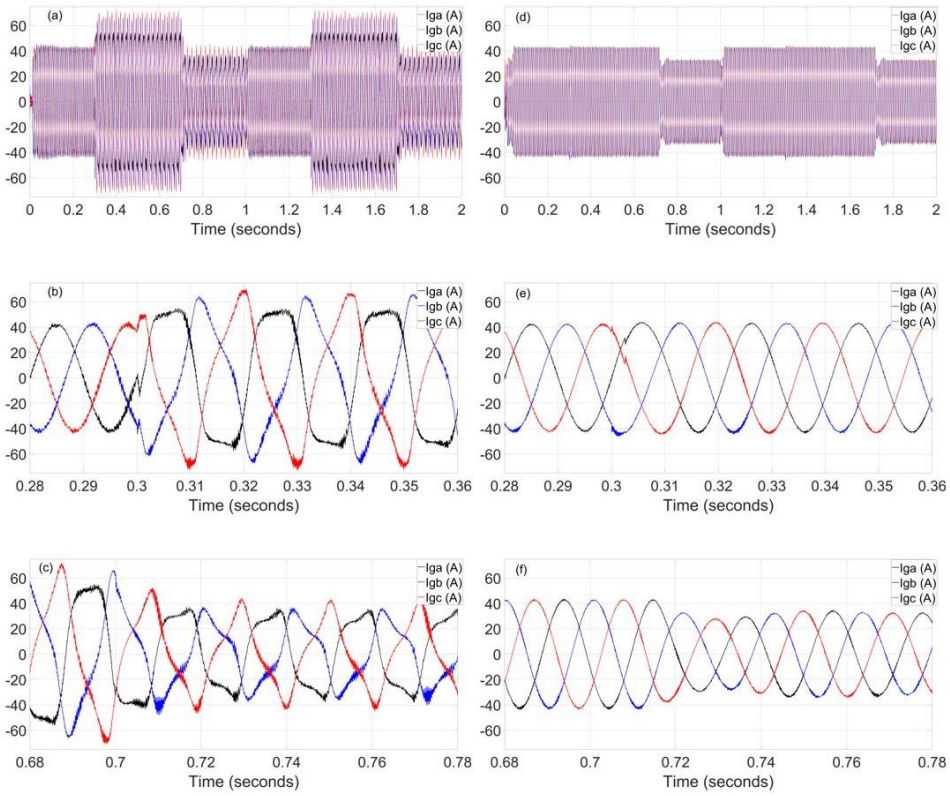

Fig. 16. Current responses injected into the grid: conventional method (a)–(c); proposed method (d)–(f)

In addition, the quality of the currents injected into the grid of the proposed method in Figs. 16(d)–16(f) is also better than that of the conventional method in Figs. 16(a)–16(c). The power ripples injected into the grid of the proposed method in Fig. 17(b) are lower than those of the conventional one in Fig. 17(a).

Moreover, the fundamental phase current magnitudes and the current THD values have also been measured in one fundamental cycle at 1.28 s, 1.48 s, 1.67 s, and 1.97 s and showed in Fig. 18 and Tables 2–3.

In the first interval, the current magnitude of the conventional method is 42.07 A as showed in Fig. 18(a), it is slightly higher than the rated value. This magnitude is also similar to that of the proposed method in Fig. 18(e). However, due to the existence of the grid voltage harmonics, THD as 1.5%, this causes the ripples in the estimated voltage magnitude of the conventional PLL in Fig. 13(b) to increase. Consequently, the current harmonics injected into the grid significantly increase in Fig. 18(a), the current THD is 3.88%. This also leads to the increase of power ripples in Fig. 17(a). In contrast to this, the proposed PLL is immune to the grid voltage harmonics. This helps the estimated voltage magnitude in Fig. 13(e) not contain the ripples. As a result, the current THD is only 1.99% in Fig. 18(e) and lower than that of the conventional PLL in Fig. 18(a). In addition, the ripples of powers in Fig. 17(b) are also lower than those in Fig. 17(a).

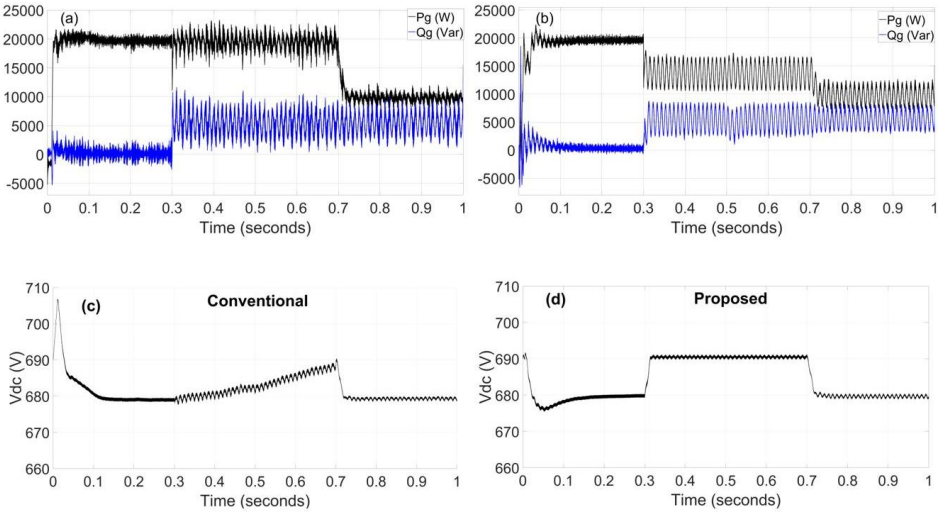

Fig. 17. Power responses injected into the grid and DC voltage: conventional method (a) and (c); proposed method (b) and (d)

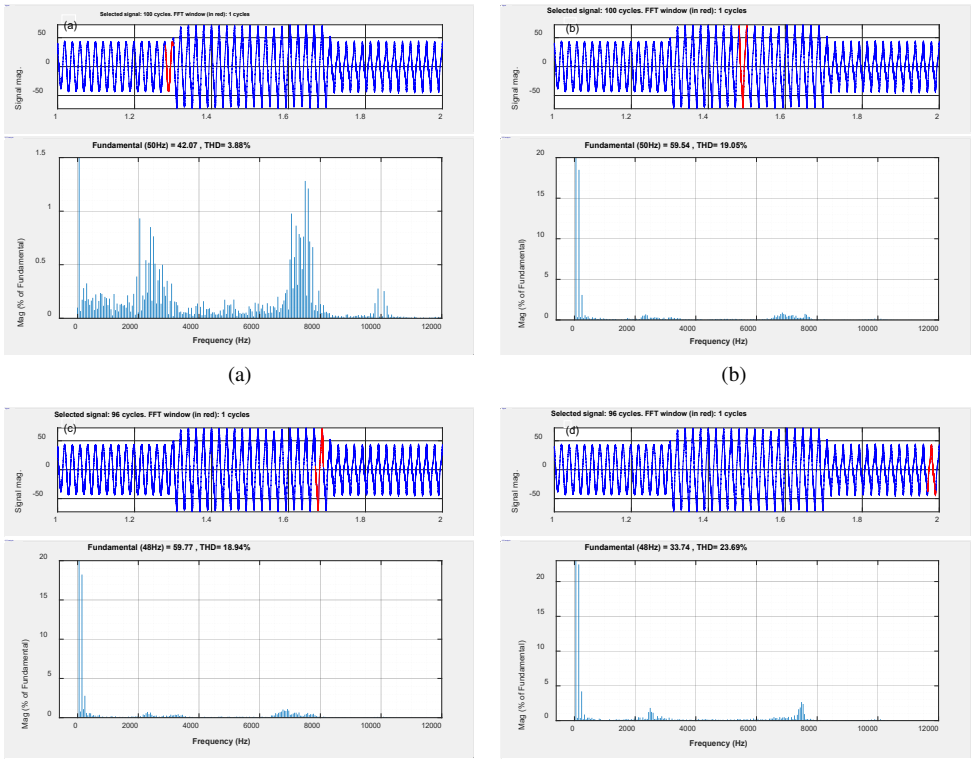

Fig. 18

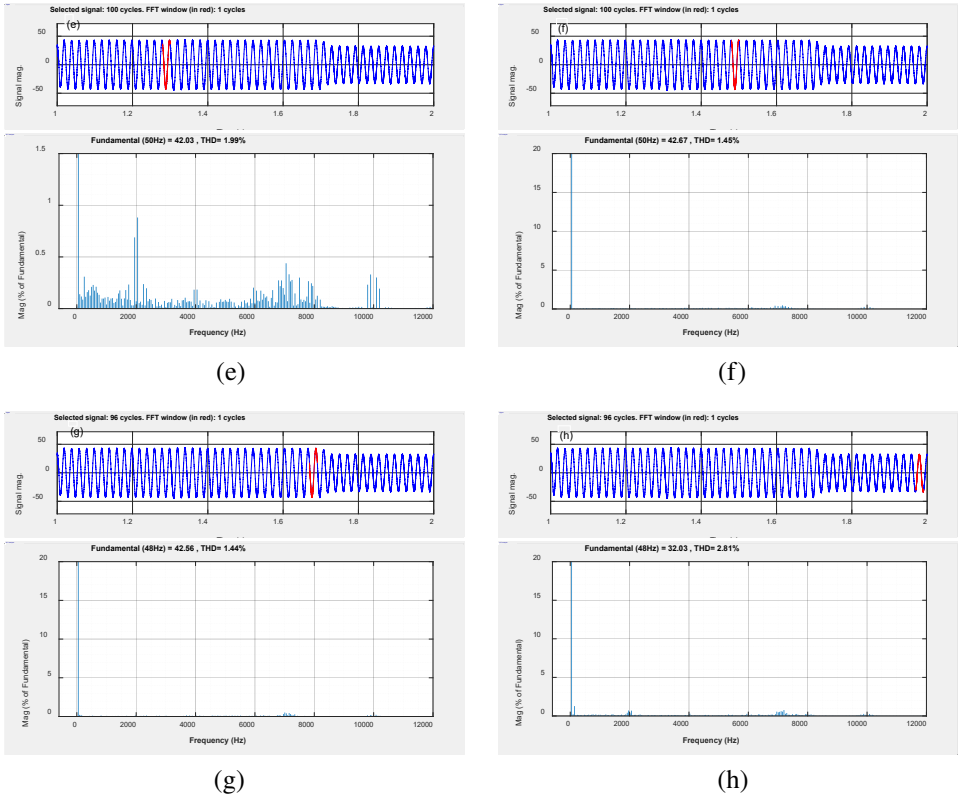

Fig. 18. Current spectra and THD values of phase C measured in one fundamental cycle at 1.28, 1.48, 1.67 s, and 1.97 s: conventional method (a)–(d); proposed method (e)–(h)

Table 3. Fundamental current magnitude and current THD of the phases A and B

At the instant (s)	Conventional method				Proposed method			
	Phase A		Phase B		Phase A		Phase B	
	***I*peak (A)**	**THD (%)**	***I*peak (A)**	**THD (%)**	***I*peak (A)**	**THD (%)**	***I*peak (A)**	**THD (%)**
1.28	42.9	3.05	42.09	3.49	42.04	**1.89**	42.06	**1.89**
1.48	60.34	18.62	56.31	19.64	42.77	**1.23**	42.61	**1.33**
1.67	60.44	17.79	56.01	19.74	42.68	**1.56**	42.53	**1.77**
1.97	34.3	24.31	30.05	27.54	32.52	**2.84**	32.76	**2.91**

In the second interval, 0.3–0.5 s (or 1.3–1.5 s), when the voltage imbalance happens after 0.3 s, the estimated voltage magnitude and frequency of the conventional PLL in Figs. 13(b)–13(c) oscillate significantly due to the effects of the negative sequence voltages and make the reference power ripples in Fig. 14(a) increase respectively. In consequence, the fundamental current mag-

www.czasopisma.pan.pl PAN POLSKA AKADEMIA NAUK www.journals.pan.pl

nitude injected into the grid increases up to 59.54 A in Fig. 18(b) and is higher than the rated current. In addition, the current THD also increases up to 19.05% and exceeds the permitted limit while the fundamental current magnitude of the proposed method in Fig. 18(f) is still 42.67 A and the current THD is only as 1.45%.

In the third interval, 0.5–0.7 s (or 1.5–1.7 s), the results of the two methods are still similar to those in the second intervals. However, during these two intervals, 0.3–0.7 s (or 1.3–1.7 s), the grid voltage magnitude drops below 90% of the rated value. The inverter needs to generate the reactive power to support the grid according to the grid codes. This makes the reference active power P_{ref} lower than the active power of the solar array P_{solar} in Fig. 14. This imbalance of active powers causes the DC voltage in Figs. 17(c)–17(d) to increase because the MPPT is still working. If this state exists for a long time, it can cause overvoltage at the DC side. Therefore, a discharge of the part of differential power needs to be implemented to balance the active power and stabilize the DC voltage. In this paper, the author suggests using a resistant load controlled by the PWM technique.

In the final interval, 07–1 s (or 1.7–2 s), the irradiance of the solar array is decreased to 500 W/m^2 and makes the solar array power P_{solar} lower than the calculated active power P_{new} Then, the reference power P_{ref} is chosen as the solar array power P_{solar}. This helps the current magnitude injected into the grid be smaller than the rated value. However, the current harmonic of the conventional method in Fig. 16(c) is higher than that of the proposed method in Fig. 16(f) and shown in Fig. 18(d) and Fig. 18(h).

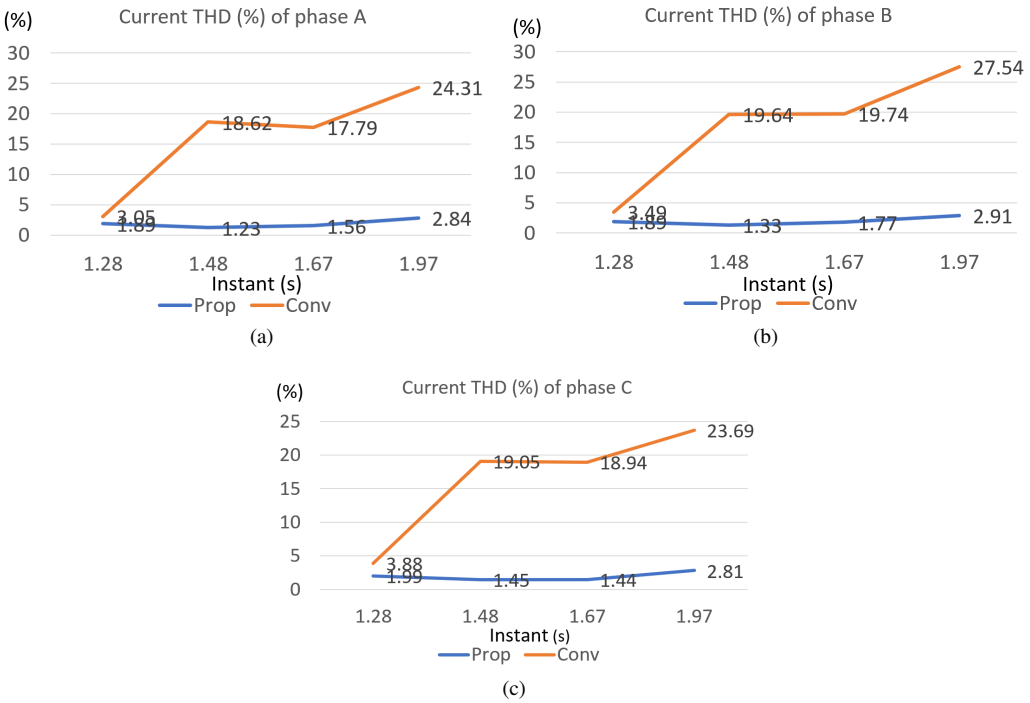

Fig. 19. Current THD curves of three phases: phase A (a); phase B (b); phase C (c)

www.czasopisma.pan.pl PAN POLSKA AKADEMIA NAUK www.journals.pan.pl

5. Conclusions

In the operation of grid-connected inverters, the faults such as voltage sag and imbalance can cause over-current in the power electronic devices and increase current harmonics injected into the grid. Based on the analysis of the voltage sequence components, this paper has proposed a method for limiting the over-current of the inverters when the voltage imbalance happens. The adverse effects of the negative sequence voltages are completely rejected by using the multiple-complex-coefficient filter in the proposed PLL. Moreover, the reference power calculation is also presented. The proposed method also helps current harmonics and power ripples injected into the grid decrease significantly. In addition, this method does not require any hardware. The simulation results on Matlab/Simulink have also been surveyed and evaluated quantitatively to validate the effectiveness of the proposed method compared with that of the conventional method.

Acknowledgments

This work belongs to the project of the year 2022 funded by Ho Chi Minh City University of Technology and Education, Vietnam.

References

[1] Chen Z., Guerrero J.M., Blaabjerg F., Member S., *A Review of the State of the Art of Power Electronics for Wind Turbines*, Transactions of Power Electronics, vol. 24, no. 8, pp. 1859–1875 (2009), DOI: 10.1109/TPEL.2009.2017082.

[2] Teodorescu R., Liserre M., Rodriguez P., *Grid Converters for Photovoltaic and Wind Power Systems* (2011).

[3] Kacejko P., Pijarski P., Gryniewicz-Jaworska M., *Generation and absorption of reactive power by wind farms – consequences of implementation of EU*, Archives of Electrical Engineering, vol. 68, no. 4, pp. 737–747 (2019), DOI: 10.24425/aee.2019.130680.

[4] Teodorescu L.R., Blaabjerg F., Liserre M., Loh P.C., *Proportional-resonant controllers and filters for grid-connected voltage-source converters*, IEE Proceedings - Electrical Power Application, vol. 153, no. 5, pp. 750–762 (2006).

[5] De Donato G., Scelba G., Borocci G., Giulii Capponi F., Scarcella G., *Fault-Decoupled Instantaneous Frequency and Phase Angle Estimation for Three-Phase Grid-Connected Inverters*, Transactions of Power Electronics, vol. 31, no. 4, pp. 2880–2889 (2016), DOI: 10.1109/TPEL.2015.2445797.

[6] Xi Z., Zhao F., Zhao X., Peng H., Xi C., *Research on islanding detection of solar distributed generation based on best wavelet packet and neural network*, Archives of Electrical Engineering, vol. 68, no. 4, pp. 703–717 (2019), DOI: 10.24425/aee.2019.130678.

[7] Wang H., *Fault diagnosis of analog circuit based on wavelet transform and neural network*, Archives of Electrical Engineering, vol. 69, no. 1, pp. 175–185 (2020), DOI: 10.24425/aee.2020.131766.

[8] Ling L.I.U., *Faulted feeder identification and location for a single line-to-ground fault in ungrounded distribution system based on principal frequency component*, Archives of Electrical Engineering, vol. 69, no. 3, pp. 695–704 (2020), DOI: 10.24425/aee.2020.133926.

[9] IEEE, *IEEE Recommended Practice for Utility Interface of Photovoltaic (PV) Systems*, IEEE Std 929–2000 (2000), DOI: 10.1109/IEEESTD.2000.91304.

[10] IEEE Standard, *IEEE P1547. 2^{TM}/D 7 Draft Application Guide for IEEE Std 1547*, Standard for Interconnecting Distributed Resources with Electric Power Systems, no. March (2007), DOI: 10.1109/IEEESTD.2011.5960751.

www.czasopisma.pan.pl PAN POLSKA AKADEMIA NAUK www.journals.pan.pl

[11] IEEE Standard, IEEE Application Guide for IEEE Std 1547(TM), *IEEE Standard for Interconnecting Distributed Resources with Electric Power Systems*, IEEE Std 1547.2-2008, no. April, pp. 1–217 (2009), DOI: 10.1109/IEEESTD.2008.4816078.

[12] Rymarski Z., Bernacki K., Dyga L., *A Control for an Unbalanced 3-Phase Load in UPS Systems*, Elektron. ir Elektrotechnika, vol. 24, no. 4 (2018), DOI: 10.5755/j01.eie.24.4.21474.

[13] Rodríguez P., Teodorescu R., Candela I., Timbus A.V., Liserre M., Blaabjerg F., *New positive-sequence voltage detector for grid synchronization of power converters under faulty grid conditions*, PESC Record - IEEE Annual Power Electronics Specialists Conference, pp. 1–7 (2006), DOI: 10.1109/PESC.2006.1712059.

[14] Rodríguez P.Ç., Luna A.Ç., Ciobotaru M.Ë., Teodorescu R.Ë., Blaabjerg F.Ë., *Advanced Grid Synchronization System for Power Converters under Unbalanced and Distorted Operating Conditions*, Proc. 32nd Ann. Conf. IEEE Ind. Elect., (IECON), no. 2, pp. 5173–5178 (2006).

[15] Zeng J., Zhang Y., *Research on optimal configuration of fault current limiter based on reliability in large power network*, Archives of Electrical Engineering, vol. 69, no. 3, pp. 661–677 (2020), DOI: 10.24425/aee.2020.133924.

[16] Wenxin Yu., Shao Dao Huang, Dan Jiang, *A fault monitoring method for wind power generation system based on sliding mode observer*, Archives of Electrical Engineering, vol. 69, no. 3, pp. 625–643 (2020), DOI: 10.24425/aee.2020.133922.

[17] Zeng R., Xu L., Yao L., Finney S.J., *Analysis and control of modular multilevel converters under asymmetric arm impedance conditions*, IEEE Trans. Ind. Electron., vol. 63, no. 1, pp. 71–81 (2016), DOI: 10.1109/TIE.2015.2477057.

[18] Guo X., Liu W., Zhang X., Sun X., Lu Z., Guerrero J.M., *Flexible control strategy for grid-connected inverter under unbalanced grid faults without PLL*, IEEE Transactions of Power Electronics, vol. 30, no. 4, pp. 1773–1774 (2015), DOI: 10.1109/TPEL.2014.2344098.

[19] Zhang Y., Qu C., *Table-Based Direct Power Control for Three-Phase AC/DC Converters under Unbalanced Grid Voltages*, IEEE Transactions of Power Electronics, vol. 30, no. 12, pp. 7090–7099 (2015), DOI: 10.1109/TPEL.2014.2387694.

[20] Hirofumi Akagi, Watanabe E.H., Mauricio Aredes, *Instantaneous Power Theory*, Instantaneous Power Theory and Applications to Power Conditioning, 2nd ed., John Wiley & Sons, Inc., pp. 37–109 (2017).

[21] Tang L., Ooi B.T., *Managing zero sequence in voltage source converter*, Conf. Rec. Annu. Meet. IEEE Ind. Appl. Soc., vol. 2, pp. 795–802 (2002), DOI: 10.1109/IAS.2002.1042650.

[22] Montanari A.A., Gole A.M., *Enhanced Instantaneous Power Theory for Control of Grid Connected Voltage Sourced Converters under Unbalanced Conditions*, IEEE Transactions on Power Electronics, vol. 32, no. 8, pp. 6652–6660 (2017), DOI: 10.1109/TPEL.2016.2627049.

[23] Hadjidemetriou L., Kyriakides E., Blaabjerg F., *Synchronization of grid-connected renewable energy sources under highly distorted voltages and unbalanced grid faults*, IECON Proc. - Industrial Electron. Conf., pp. 1887–1892 (2013), DOI: 10.1109/IECON.2013.6699419.

[24] Hadjidemetriou L., Kyriakides E., Blaabjerg F., *A Robust Synchronization to Enhance the Power Quality of Renewable Energy Systems*, IEEE Trans. Ind. Electron., vol. 62, no. 8, pp. 4858–4868 (2015), DOI: 10.1109/TIE.2015.2397871.

[25] Guo X., Wu W., Chen Z., *Multiple-complex coefficient-filter-based phase-locked loop and synchronization technique for three-phase grid-interfaced converters in distributed utility networks*, IEEE Trans. Ind. Electron., vol. 58, no. 4, pp. 1194–1204 (2011), DOI: 10.1109/TIE.2010.2041738.

[26] Maurya G.K., Verma A.K., Subramanian C., Sharma B.B., *Fixed-Frequency MCCF Based Grid Synchronization Technique*, Proc. 2018 IEEE Int. Conf. Power Electron. Drives Energy Syst. PEDES 2018, pp. 1–4 (2018), DOI: 10.1109/PEDES.2018.8707552.

www.czasopisma.pan.pl PAN POLSKA AKADEMIA NAUK www.journals.pan.pl

[27] Shuvra M.A., Member S., Charlotte U.N.C., *Selective Harmonic Compensation by Smart Inverters using Multiple-Complex-Coefficient-Filter (MCCF) during Unbalanced Fault Condition* (2017).

[28] Kumar R., Sahu B., Shiva C.K., Rajender B., *A control topology for frequency regulation capability in a grid integrated PV system*, Archives of Electrical Engineering, vol. 69, no. 2, pp. 389–401 (2020), DOI: 10.24425/aee.2020.133033.

[29] Das J.C., *Chapter 8. Effects of Harmonics*, Power System Harmonics and Passive Filter Designs, New Jersey: John Wiley & Sons, pp. 331–378 (2015).

[30] Guo X., Guerrero J.M., *Abc-frame complex-coefficient filter and controller based current harmonic elimination strategy for three-phase grid connected inverter*, J. Mod. Power Syst. Clean Energy, vol. 4, no. 1, pp. 87–93 (2016), DOI: 10.1007/s40565-016-0189-4.

[31] Li Y., Yang R., Zhao X., *Reactive power convex optimization of active distribution network based on Improved Grey Wolf Optimizer*, Archives of Electrical Engineering, vol. 69, no. 1, pp. 117–131 (2020), DOI: 10.24425/aee.2020.131762.

[32] Ji L. *et al.*, *A Multi-objective Control Strategy for Three Phase Grid-Connected Inverter during Unbalanced Voltage Sag*, IEEE Transactions of Power Delivery (2020), DOI: 10.1109/TPWRD.2020.3025158.

[33] Rodríguez P., Pou J., Bergas J., Candela J.I., Burgos R.P., Boroyevich D., *Decoupled double synchronous reference frame PLL for power converters control*, IEEE Transactions of Power Electronics, vol. 22, no. 2, pp. 584–592 (2007), DOI: 10.1109/TPEL.2006.890000.